Polyhedron 257 (2024) 117011

Contents lists available at ScienceDirect

Polyhedron

journal homepage: www.elsevier.com/locate/poly

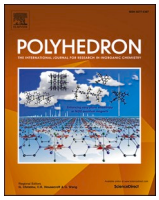

New silver, rhodium and iridium complexes with anthracene-functionalized *N*-heterocyclic carbene ligands: Crystal structures, cytotoxicity and fluorescence studies

Hatice Bekci [a], Namık Özdemir [b], Zeynel Şahin [c], Akın Mumcu [d], Serkan Dayan [e,*], Mert Olgun Karataş [f,*]

[a] *Develi Hüseyin Şahin Vocational School, Kayseri University, Kayseri, Turkey*
[b] *Department of Mathematics and Science Education, Faculty of Education, 9055139 Samsun, Turkey*
[c] *Department of Material Engineering, Faculty of Engineering, Marmara University, 9034722 İstanbul, Turkey*
[d] *Scientific and Technological Research Center, İnönü University, 9044280 Malatya, Turkey*
[e] *Drug Application and Research Center, Molecular Synthesis and Industrial Application Laboratory (MSIA-Lab), Erciyes University, Kayseri, Turkey*
[f] *Department of Chemistry, Faculty of Science, İnönü University, 9044280 Malatya, Turkey*

ARTICLE INFO

Keywords:
Benzimidazole
Anthracene
N-heterocyclic carbene
Silver
Rhodium
Iridium
Fluorescence
Cytotoxicity

ABSTRACT

In the present study, we have synthesized anthracene-functionalized metal complexes to investigate their cytotoxicity and photophysical properties. In this context, firstly, an Ag–NHC (NHC = *N*-heterocyclic carbene) complex (**2a**) has been synthesized by the interaction of Ag_2O and *N*-(2-methylbenzyl)-*N*-((anthracen-9-yl) methyl)benzimidazolium chloride (**1a**). Corresponding Rh– (**3a**) and Ir–NHC (**4a**) complexes have also been synthesized by the transmetalation reaction between 2a and corresponding metal compounds. Additionally, for comparison purposes, an ether-functionalized Ag–NHC complex (**2b**) with *N*-(methoxyethyl)-*N*-((anthracene-9-yl)methyl)benzimidazole-2-ylidene ligand, and $[AgL_2]NO_3$ type complex (**2c**) with a *N*-coordinated *N*-((anthracen-9-yl)methyl)benzimidazole ligand have been synthesized. All complexes have been characterized by the combination of NMR and mass spectroscopic techniques, and elemental analyses. Moreover, solid state structures of **2a**, **2b** and **4a** have been determined by the single crystal X-ray diffraction analysis. Cytotoxic potentials of all compounds have been tested against human lung adenocarcinoma alveolar basal epithelial cell line (A549) using the MTT assay, and all complexes performed strong anti-proliferative activity. Stability studies have disclosed that only **1a** and **2c** are able to retain their structure in the culture medium (DMEM) that biological assays were carried out. Photophysical measurements revealed that all compounds have similar emission bands because of the conjugation of anthracene group. Finally, **1a** and **2c** have been visualized by fluorescence confocal microscopy to investigate cellular uptake and subcellular distribution of the complexes, and the findings indicated that both compounds dispersed along the cell membranes nuclear regions.

1. Introduction

The medical applications of metal compounds trace back to ancient times, but their investigation as modern therapeutic agents began after the discovery of cisplatin in 1965 [1]. The coordination numbers of metal atoms ranging from two to ten allow the metal complexes to have various geometric structures, and this feature, which is impossible to achieve with organic compounds, paves the way for unique interactions with biomolecules [2]. Moreover, introducing the organic ligands, whose carbon scaffold can be modified, to the structure of metal complexes makes it possible to prepare an unlimited number of metal complexes. The nature of the ligand is quite decisive on the electronic and steric properties of the complex, and *N*-heterocyclic carbenes (NHCs), which are a class of neutral carbon compounds, are one of the mostly used class of ligands in organometallic chemistry. Metal-NHC complexes have found wide application in the fields of catalysis and medicinal chemistry, thanks to their two advantages over other organic ligands; first, NHCs are strong σ–donor ligands, able to form strong metal–carbon bond, and therefore produce highly stable metal complexes, second, the carbon scaffold of NHC ligands can be easily

* Corresponding authors.
E-mail addresses: serkandayan@erciyes.edu.tr (S. Dayan), mert.karatas@inonu.edu.tr (M.O. Karataş).

https://doi.org/10.1016/j.poly.2024.117011
Received 19 February 2024; Accepted 26 April 2024
Available online 27 April 2024

modified for specific requirements [3].

Increased stability in aqueous solution and test medium that biological assay was carried out are highly important for a drug candidate, and thanks to their high stability, numerous NHC complexes have been reported for biological purposes with both noble and earth-abundant metals [4]. Furthermore, "switchable" or "multifunctional" metal-NHC complexes can be easily prepared by the attaching the responsive group to NHC scaffold [5]. For example, metal-NHC complexes that are responsive to stimuli such as light [6] or pH [7] can be prepared by the attaching the responsive group to NHC scaffold. Also, metal-NHC complexes with enhanced biological activity and bio-conjugation can be prepared by the attaching biologically-relevant group to NHC scaffold [8].

The attachment of a fluorophore group to a drug is a new strategy to trace them in cells [9], and this approach has also successfully been applied for metal-NHC complexes [10]. Silver [10a,b,e,f], gold [10b,c,d,f], rhodium [10 g,h] and ruthenium [10] complexes with anthracene-[10a,e,f,g], pyridine- [10], coumarin- [10] or naphthalimide-functionalized [10d,h] NHC ligands have been used to learn more information on distribution of metal-NHC complexes in human ovarian, breast, colon and neuroblastoma cancer cell lines. Among these fluorophores, anthracene comes into prominence because of relatively easier preparation of anthracene-functionalized complexes, and therefore, more anthracene-functionalized metal-NHC complexes have been reported with promising biological activity [11]. On the other hand, *N*-flanking anthracenyl moiety in NHC ligands can be classified as "non-innocent" group. In a recent study, Hartinger and co-workers reported that a incorporation of a *N*-substituted anthracenyl moiety to [Rh(Cp)(NHC)Cl_2] (Cp = cyclopentadienyl) type complex led to the formation of heptadentate and octadentate all-carbon atom ligands [12]. The most recently, Han and co-workers reported the [4 + 4] photodimerization of silver and gold complexes with anthracene-functionalized NHC ligands under irradiation at 365 nm [13].

Following the promising results obtained with anthracenyl-functionalized NHC complexes, in the present study, we aimed to develop anticancer metal complexes that are decorated with anthracenyl moiety with good stability in test medium and fluorescence emission for bio-imaging. For this purpose, in the first step, we prepared silver, rhodium and iridium complexes of N-(2-methylbenzyl)-N-((anthracen-9-yl)methyl)benzimidazol-2-ylidene ligand. Later, we prepared a silver-NHC complex with N-(2-methoxyethyl)-N-((anthracen-9-yl)methyl)benzimidazol-2-ylidene and a *N*-coordinated silver complex with N-((anthracen-9-yl)methyl)benzimidazole for comparison purposes.

2. Results and discussion

2.1. Synthesis and characterization of the complexes

In the first step, N-(2-methylbenzyl)-N-((anthracen-9-yl)methyl) benzimidazolium chloride (**1a**) was synthesized according to the procedure described in our previous study [14]. The Ag–NHC complex (**2a**) of this ligand was synthesized by the reaction of Ag_2O and **1a** in methylene chloride. Rh–NHC (**3a**) and Ir–NHC (**4a**) complexes were synthesized by the transmetalation reaction between **2a**, and [RhCl(COD)]$_2$ and [IrCl(COD)]$_2$ (COD = cyclooctadiene), respectively. Later, in order to synthesize an ether-functionalized Ag–NHC with improved solubility, we synthesized N-(2-methoxyethyl)-N-((anthracen-9-yl)methyl)benzimidazolium chloride (**1b**) according to procedure described in our previous study [14], and deprotonation of **1b** by Ag_2O in DCM yielded **2b**. Lastly, we synthesized a silver complex with *N*-coordinated ligand for comparison purposes. N-(((anthracen-9-yl)methyl) benzimidazole) (**1c**) was synthesized according to the procedure described in literature [10], and its [AgL_2](NO_3) type complex (**2c**) was synthesized by the interaction of **1c** and $AgNO_3$ in ethanol. Structures, synthesis and yields of all complexes are outlined in Schemes 1, 2 and 3.

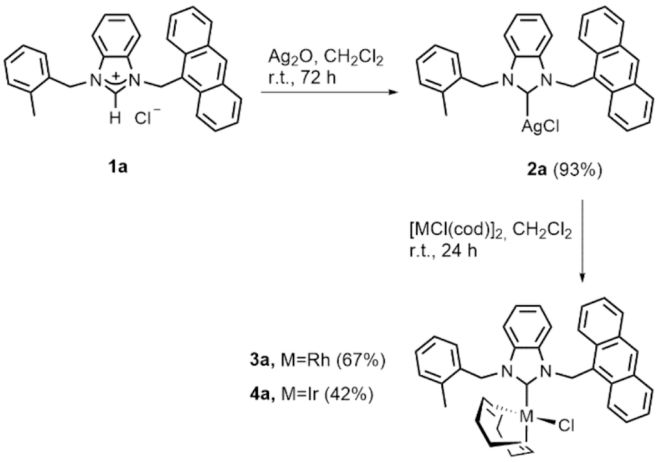

1a 2a (93%)

Scheme 1. Synthesis and structure of **2a**-**4a**.

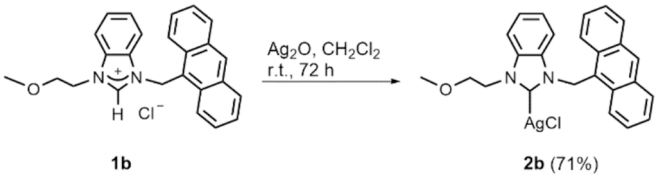

1b 2b (71%)

Scheme 2. Synthesis and structure of **2b**.

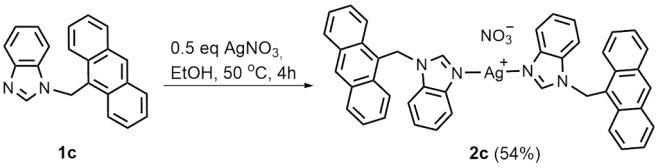

1c 2c (54%)

Scheme 3. Synthesis and structure of **2c**.

We must note that all complexes were synthesized under open-air conditions and in the absence of the light. All complexes are highly stable in solid state against oxygen and moisture, and silver complexes, **2a-c**, were stored in dark.

The complexes were characterized by the combination of NMR and mass spectroscopy, and elemental analyses. Additionally, solid state crystal structures of **2a**, **2b** and **4a** were determined by single crystal X-ray analysis.

In the ^{1}H NMR spectrum of **2a**, the signal of acidic –NCHN– hydrogen, which had been observed at 9.25 ppm, disappeared completely. The signals of the aromatic hydrogens were observed in the range of 8.64–6.62 ppm, in the expected integral values. The signal of methylene hydrogens connecting the imidazole and anthracene moieties was observed as a singlet at 6.57 ppm, while the signal of methylene hydrogens between imidazole and phenyl moieties was observed as a singlet at 5.57 ppm. The signal of methyl hydrogens was observed as a singlet at 2.34 ppm. In the ^{13}C NMR spectrum of **2a**, the signal of –NCHN– carbon, which had been observed at 142.5 ppm, disappeared completely, but the signal of carbene carbon could not been detected due to labile nature of Ag–C bond. The signals of aromatic carbons were observed in the range of 135.4–112.1 ppm. The methylene carbon connecting imidazole and anthracene moieties was observed at 51.9 ppm, while the methylene carbon between imidazole and phenyl moieties was observed at 47.1 ppm. The methyl carbon was observed at 19.6 ppm. LC-MS spectrum of **2a** in DMSO showed that the complex has bis-NHC structure with [Ag(NHC)$_2$](AgCl$_2$) formula in solution.

In the ^{1}H NMR spectrum of **2b**, the signal of acidic –NCHN–

hydrogen, which had been observed at 9.11 ppm, disappeared completely. The signals of aromatic hydrogens were observed in the range of 8.75–7.37 ppm, in the expected integral values. The signal of methylene hydrogens between imidazole and anthracene moieties was observed as a singlet at 6.49 ppm. Totally four hydrogens of two methylene carbons belonging to ether group were observed as two separate multiplets at 4.35 and 3.58 ppm, while the signal of methyl hydrogens were observed as a multiplet at 3.05 ppm. In the ^{13}C NMR spectrum of **2b**, the signal of –NCHN– carbon, which had been observed at 142.3 ppm, disappeared completely, and the signal of the carbene carbon was observed at 188.4 ppm. The signals of aromatic carbons were observed in the range of 134.3–112.5 ppm. The methylene carbon connecting the imidazole and anthracene moieties was observed at 49.5 ppm. The methylene carbons belonging to ether group were observed at 71.1 and 58.7 ppm, and the methyl carbon was observed at 45.3 ppm. LC-MS spectrum of **2b** in DMSO showed that the complex has bis-NHC structure with $[Ag(NHC)_2](AgCl_2)$ formula in solution.

In the ^{1}H NMR spectrum of **2c**, the –NCHN– hydrogen was observed at 7.86 ppm, as a singlet. The signals of aromatic hydrogens were observed in the range of 8.82–7.35 ppm, in the expected integral values and coupling patterns. The signal of methylene hydrogens between imidazole and anthracene moieties was observed as a singlet at 6.57 ppm. In the ^{13}C NMR of **2c**, the signal of –NCHN– carbon was observed at 144.9. The number of signals detected in aromatic region (141.6–112.2 ppm) matched the numbers of different carbon atoms expected from the structure. The methylene carbon connecting the imidazole and anthracene moieties was observed at 41.9 ppm. In addition to elemental analysis, LC-MS spectrum of **2c** in DMSO also supported the *N*-coordination of ligand that yields $[Ag(L)_2]NO_3$ type complex. Despite our all attempt, we could not obtain suitable crystals for single-crystal X-ray analysis for **2c**, however, the proposed structure by the combination of NMR and mass spectroscopy and elemental analysis techniques are consistent with literature [15].

In the ^{1}H NMR spectrum of **3a**, the diastereotopic methylene hydrogens between imidazole and anthracene moieties were observed as overlapped with aromatic hydrogens around 7.6 and 6.8 ppm. The other methylene hydrogens connecting imidazole and phenyl moieties were also observed as diastereotopic hydrogens around 6.8 and 5.8 ppm with 16.6 Hz of coupling constant. The four olefinic COD hydrogens were observed as multiplets at 5.32, 3.64 and 2.65 ppm. The remaining aromatic and aliphatic hydrogens were observed in expected integral values. In the ^{13}C NMR spectrum of **3a**, the signal of carbene carbon was observed as a doublet at 197.8 ppm with 51.0 Hz of $J_{Rh\text{-}C}$ coupling constant. The olefinic carbons of COD that are coordinated to Rh center were also observed as doublets, at 100.5, 100.4, 70.3 and 68.7 ppm with 6.6 and 14.3 Hz of $J_{Rh\text{-}C}$ coupling constants. The methylene carbon connecting imidazole and anthracene moieties were observed at 50.4, while the methylene carbon between imidazole and phenyl moieties were observed at 48.2 ppm. The number of signals detected in aromatic and aliphatic regions exactly matched the numbers of the remaining aromatic and aliphatic carbons expected from the structure. LC-MS spectrum of the complex in DMSO showed that the complex has [Rh(NHC)Cl] structure in solution.

In the ^{1}H NMR spectrum of **4a**, one of the diastereotopic methylene hydrogens between imidazole and anthracene moieties was observed as a doublet at 6.61 ppm with 15.1 Hz of coupling constant, while the other was observed as overlapped with aromatic hydrogens around 7.4 ppm. The other methylene hydrogens that are between imidazole and phenyl moieties were observed similarly, one was observed as overlapped with aromatic hydrogens around 6.4 ppm, while the other was observed as a doublet at 5.69 ppm with 16.5 Hz of coupling constant. The four olefinic COD hydrogens were observed as multiplets at 4.75, 3.24 and 2.89 ppm. The remaining aromatic and aliphatic hydrogens were observed in expected integral values. In the ^{13}C NMR spectrum of **4a**, the signal of carbene carbon was observed at 193.1 ppm. The four olefinic COD carbons that are coordinated to Ir center were observed at 87.5, 87.4, 54.0, 52.4 ppm. The methylene carbon connecting the imidazole and anthracene moieties was observed at 50.0, while the methylene carbon between imidazole and phenyl moieties was observed at 47.9 ppm. The signals of remaining aromatic and aliphatic hydrogens were observed in the expected integral values. LC-MS spectrum of the complex in DMSO showed that the complex has [Ir(NHC)Cl] structure in solution.

2.2. Crystal structure description

The molecular structures of **2a**, **2b** and **4a** were determined by single-crystal X-ray diffraction studies and shown in Fig. 1. All the compounds crystallize in the triclinic space group $P-1$ with two molecules in the unit cell. Important bond lengths and angles of the compounds are listed in Table 1.

X-ray studies of **2a** and **2b** prove the formation of neutral (NHC)Ag-Cl type monomeric complexes without argentophilic Ag···Ag interactions. The silver atoms are coordinated by the carbenic carbon of the NHC ligand and a chloride ion, and deviate significantly from linearity with C—Ag—Cl angles ranging from 171.61(5) to 173.72(7)°. The Ag—Cl and Ag—C distances changing from 2.3167(8) to 2.3276(6) Å and from 2.0913(18) to 2.092(3) Å, respectively, lie within the range usually found for (NHC)Ag-Cl complexes [16]. The dihedral angle between the mean planes of benzimidazole and anthracene rings is 80.58(11)° in **2a** and 80.49(6)° in **2b**. Furthermore, the benzene ring makes dihedral angles of 85.91(14) and 66.84(13)° with the mean planes of benzimidazole and anthracene rings, respectively.

The asymmetric unit of **4a** consists of one complex molecule and a half hexane molecule in the asymmetric unit. The coordination of the metal atom is a slightly distorted quasi-square-planar, considering the mid-points of the 1,2 and 5,6 bonds of the cycloocta-1,5-diene (COD) ligand as the donors. The metal center is coordinated to the two alkene bonds of COD ligand, to a carbenic carbon atom of the NHC ligand and to a chloride atom. For quantitative evaluation of the extent of distortion around the metal centers, the four-coordinate structural indexes τ_4 [17] and τ_4' [18] were employed;

$$\tau_4 = \frac{360^\circ - (\alpha+\beta)}{360^\circ - 2\theta}\tau_4' = \frac{\beta-\alpha}{360^\circ-\theta} + \frac{180^\circ-\beta}{180^\circ-\theta}$$

where α and β ($\beta > \alpha$) are the two greatest valence angles and θ is the ideal tetrahedral angle (109.5°). The τ_4 and τ_4' values for ideal square-planar and tetrahedral coordination spheres are 0 and 1, respectively. The calculated τ_4 and τ_4' geometry indices are both 0.03, indicating a slightly distorted square-planar geometry. The coordination plane is almost pseudo-perpendicular to the carbene heterocycle plane with a dihedral angle of 81.49(9)°. Besides, the benzimidazole ring makes dihedral angles of 77.35(16) and 79.91(9)° with the mean planes of benzene and anthracene rings, respectively.

The COD ring exhibits a boat conformation with the Ir—C_{COD} distances ranging from 2.101(3) to 2.180(3) Å. The C=C bond of the COD in a *trans*-position to the NHC ligand [1.385(6) Å] is significantly shorter and displays longer Ir—C_{COD} distances than the C=C bond *trans* to chloride [1.407(5) Å]. This indicates a strong *trans*-influence of the NHC ligands and considerably weaker coordinative bond of C=C *trans* to the NHC ligand than *trans* to chloride. The Ir—Cl bond distance is 2.3574(9) Å, and the coordination bond lengths and angles are in line with those of other [IrCl(COD)(NHC)] complexes [19].

In all compounds, the fact that N1—C1 and N2—C1 bonds are notably shorter than N1—*C*2 and N2—C7 bonds is an indicator of delocalization within the benzimidazole rings. The internal N—C—N ring angle at the carbene centers falls in the range 105.6(2)-106.2(2)°.

2.3. Photophysical properties

Photophysical properties of **1a** and all metal complexes were investigated in the DMSO solution at the same concentrations Fig. 2. The

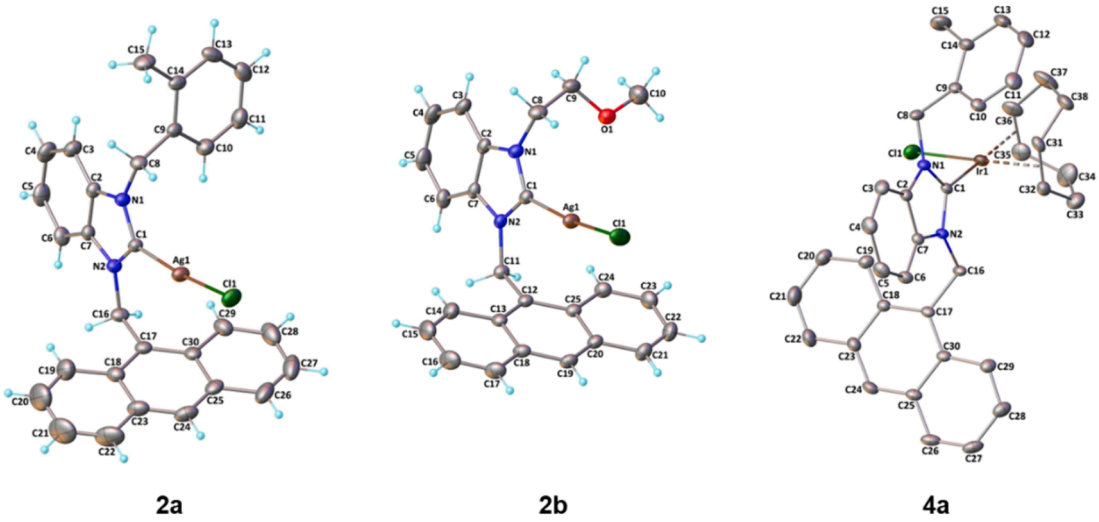

Fig. 1. Crystral structures of **2a**, **2b** and **4a**.

Table 1
Selected geometric parameters for **2a**, **2b** and **4a**.

Parameters	2a	2b	4a
Bond lengths (Å)			
M—Cl1	2.3167(8)	2.3276(6)	2.3574(9)
M—C1	2.092(3)	2.0913(18)	2.028(3)
M—C31	–	–	2.113(3)
M—C32	–	–	2.101(3)
M—C35	–	–	2.180(3)
M—C36	–	–	2.177(3)
M—ct1	–	–	1.986(3)
M—ct2	–	–	2.066(3)
N1—C1	1.349(3)	1.361(2)	1.361(3)
N1—C2	1.391(3)	1.385(2)	1.394(4)
N2—C1	1.346(3)	1.347(2)	1.360(3)
N2—C7	1.392(3)	1.399(2)	1.385(3)
Bond angles (°)			
Cl1—M—C1	173.72(7)	171.61(5)	90.58(8)
M—C1—N1	123.68(19)	123.65(13)	126.27(18)
M—C1—N2	130.09(19)	130.16(13)	128.13(19)
Cl1—*M*—ct1	–	–	177.38(6)
Cl1—*M*—ct2	–	–	90.19(10)
Cl1—*M*—C31	–	–	160.32(10)
Cl1—*M*—C32	–	–	160.35(10)
Cl1—*M*—C35	–	–	91.05(12)
Cl1—*M*—C36	–	–	89.30(12)
C1—*M*—ct1	–	–	92.05(10)
C1—*M*—ct2	–	–	178.25(13)
C1—*M*—C31	–	–	92.37(11)
C1—*M*—C32	–	–	91.47(12)
C1—*M*—C35	–	–	162.96(13)
C1—*M*—C36	–	–	159.94(14)
ct1—*M*—ct2	–	–	87.19(11)
N1—C1—N2	106.2(2)	106.14(15)	105.6(2)

UV–visible spectra were recorded in the range between 250 nm to 450 nm wavelength, and absorption bands are shown in Fig. 2A. The complexes exhibit a similar absorption spectrum, with a strong band around 260 nm and a weak band around 370 nm. Because of the conjugation the anthracene groups, the complexes have four additional peaks are observed between 330 and 400 nm in the UV–visible spectrum as mentioned in the literature [10]. Emission spectra for the complexes were obtained by exciting them at 370 nm. Complexes display similar three emission bands that two main and one weak peak at around 398, 421, and 445 nm, respectively Fig. 2B. There is no significant shifting between **1a** and all metal complexes in the emission spectrum. When we compare the emission intensities of the complexes with the highest **2c** and lowest **3a** intensity, complex **2c** is intense more than twenty-three times of complex **3a**. Excitation spectra were measured for complexes by fixing the emission wavelength at 420 nm. The excitation spectrum of each complex is identical to its corresponding absorption spectrum Fig. 2C. However, the excitation spectrum of **2c** shows inconsiderable blue-shifting as in absorption spectra. The combined emission, absorption, and excitation spectra at the 300–500 nm region of the electromagnetic spectrum of complex **2c** (as an example) are shown in Fig. 2D. The emission spectrum is a typical mirror image of the absorption spectrum. In addition, the complex showed Stokes shift of 49 nm at the UV–visible spectrum.

2.4. Cytotoxicity studies

The cytotoxicity of six compounds (**1a**, **2a**, **3a**, **4a**, **2b**, **2c**) were assessed against the human lung adenocarcinoma alveolar basal epithelial cell line A549 using the MTT assay. After a 24-hour exposure to the compound solutions, the cellular morphology changes were observed using an inverted microscope, and cell viability was determined spectrophotometrically following a predefined protocol. The cytotoxicity results have been depicted graphically as cell viability (Fig. 3). The half-maximal inhibitory concentration (IC50) values for the compounds (**1a**, **2a**, **3a**, **4a**, **2b**, **2c**) at 24 h were calculated as 3.71 μM, 5.51 μM, 5.34 μM, 5.65 μM, 5.27 μM, and 5.83 μM, respectively. To estimate the IC50 values, a common approach involves fitting the experimental data to a dose–response curve using linear regression. For this purpose, the x-y data representing compound concentrations and corresponding cell viability percentages are plotted, and a straight line is fitted to the data. The equation of the fitted line is expressed as $Y = a * X + b$, where Y represents the response (cell viability), X represents the concentration of the compound, and 'a' and 'b' are coefficients. The IC50 value can then be calculated from the equation as $(0.5 - b)/a$.

Both cell viability results and IC50 calculations revealed that **1a**, only organic compound tested, has stronger cytotoxic effect compared to all complexes. In particular, only **1a** performed remarkable cytotoxicity at 7.812 μM, and this outcome can be attributed to better solubility gained by the ionic structure. When the results of the complexes are compared, it is possible to say that all complexes have approximately the same level of cytotoxicity.

2.5. Stability studies

In order for drug candidates to perform their own activity in the biological assays, they must be soluble and stable in the test medium in which the assay was carried out. In this context, we tested the stability of

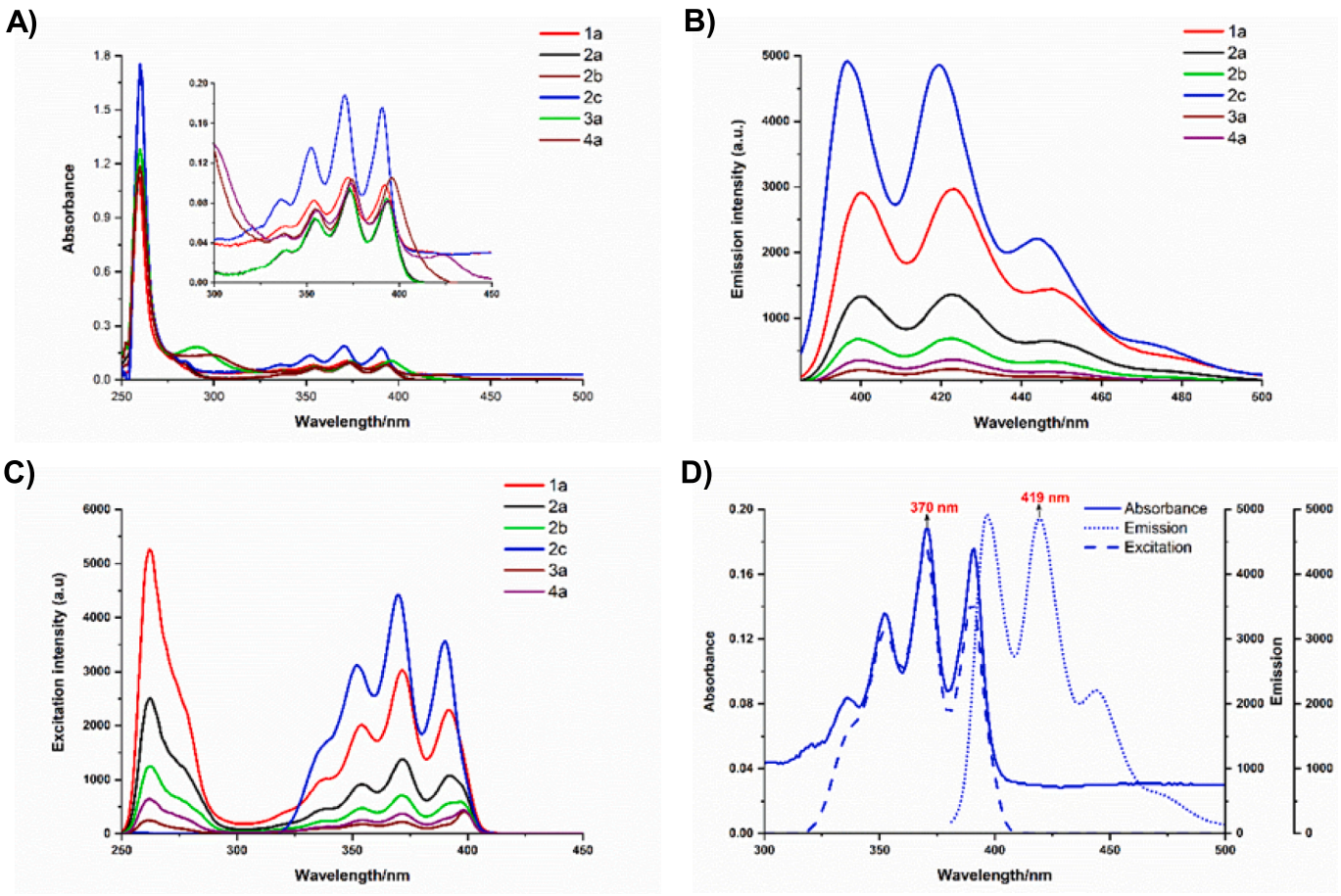

Fig. 2. Measurement for the complexes were obtained in DMSO solution at $2x10^{-6}$ M concentration under the same conditions. (A) The UV–visible spectra, (B) the emission spectra, (C) the excitation spectra, (D) overlapped absorption (λ_{max} 370 nm), emission (λ_{em} 419 nm) and excitation (λ_{ex} 370 nm) spectra of complex **2c**.

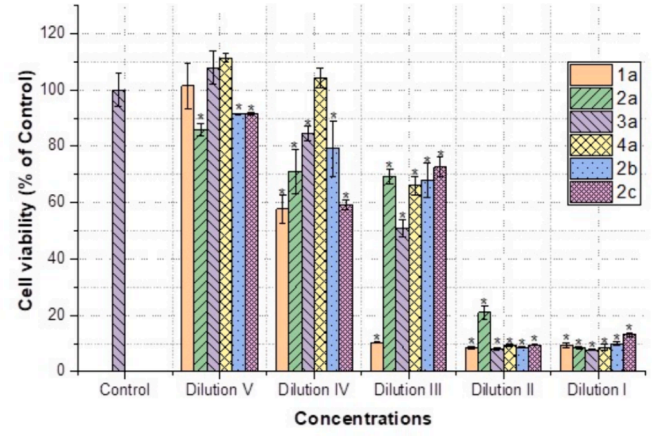

Fig. 3. Cell viability of A549 cells after 24 h incubation in the presence of **1a** – **4a**, **2b**, **2c** compounds at different dilution values (I: 62.500 μM, II: 31.250 μM, III: 7.812 μM, IV: 3.906 μM, V: 1.953 μM).

all compounds whose cytotoxicity was examined in this study for 24 h in the culture medium (DMEM). The results disclosed that only **1a** and **2c** can save their stability for 24 h and remain intact (Fig. 4). While partial degradation products were observed in complexes **2b**, **3a** and **4a**, complex **2a** was observed to be completely degraded.

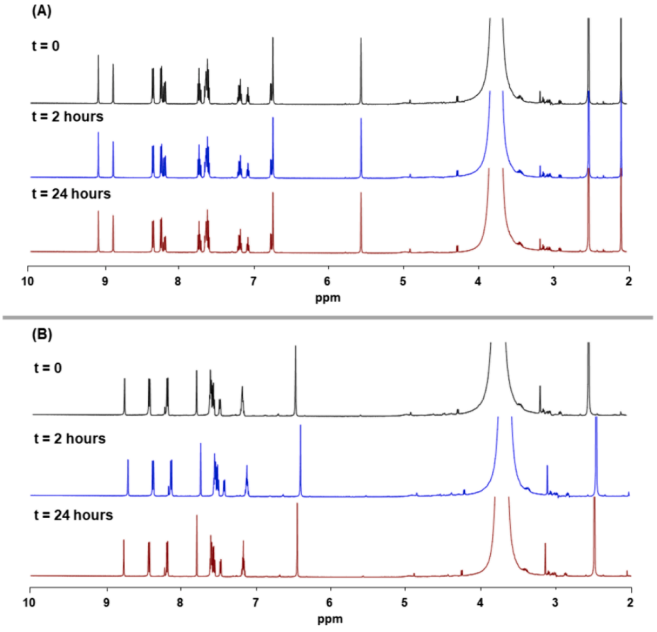

Fig. 4. (A) ^{1}H NMR spectra of **1a** in 400 mL DMSO-d_6 at different time intervals in the presence of 100 mL of culture medium (DMEM). (B) ^{1}H NMR spectra of **2c** in 400 mL DMSO-d_6 at different time intervals in the presence of 100 mL of culture medium (DMEM).

2.6. Fluorescence microscopy

The gaining deeper mechanistic insights requires understanding the cellular uptake and distribution of the tested drug candidate. Therefore, we used fluorescence confocal microscopy to investigate subcellular distribution of the compounds tested in this study. For this purpose, we chose the ligand precursor **1a** and complex **2c**, considering their higher emission intensity and excellent stability in test medium, and relatively higher cytotoxicity of **1a**. Compound **1a** and complex **2c**, each at a concentration of 15.625 μM, were incubated with the A549 cell line at 37 °C for 2 h, followed by the analysis of cellular images. Through this examination, it was distinctly observed that both compounds dispersed along the cell membranes and accumulated within the nuclear regions beyond the cell membrane (Fig. 5). Importantly, such fluorescence signals were not detected in the control cells. These findings indicate that the effects of the compounds occur not only at the cytoplasmic level but also at the nuclear level.

3. Conclusion

In summary, we have reported the synthesis and characterization of Ag–, Rh– and Ir–NHC complexes of a *N*-(2-methylbenzyl)-*N*-((anthracen-9-yl)methyl)benzimidazole-2-ylidene ligand, an Ag–NHC complex of *N*-(methoxyethyl)-*N*-((anthracen-9-yl)methyl)benzimidazole-ylidene ligand, and a *N*-coordinated $[AgL_2]NO_3^-$ type silver complex with *N*-((anthracen-9-yl)methyl)benzimidazole ligand. The anti-proliferative assays revealed that all compounds have remarkable activity against A549 cells at the 62.50 and 31.25 μM concentration levels, however we must emphasize that the cytotoxicity of the complexes are lower compared to standard drug cisplatin [20]. Stability studies disclosed that only **1a** and *N*-coordinated silver complex, **2c**, are able to retain their stability in the test medium, among the tested compounds. Furthermore, it is possible to trace **1a** and **2c** in the cell by fluorescence microscopy owing to their high fluorescence emission intensity. Although, strong cytotoxicity, excellent stability in test medium and utilization in fluorescence microscopy render **1a** and **2c** as promising anticancer agents, and we think that all compounds reported in this study deserve further mechanistic investigations owing to their promising and useful properties.

4. Experimental section

4.1. Synthesis and spectroscopic measurements

4.1.1. General remarks

The complexes were synthesized under open-air conditions. The reagents and solvents were purchased from commercial sources and used without further purification. Melting points were determined in open capillary tubes and were uncorrected, using Gallenkamp MPD350. BM3.5. C, H and N analyses were carried out using LECO CHNS-932 elemental analyser. ^{1}H and ^{13}C NMR spectra were recorded on Bruker Ascend^{TM} 400 Avance III HD. Chemical shifts are expressed in parts per million (ppm) and referenced to residual solvent peaks. Coupling constants, *J*, are given as Hz. Absorption spectra were measured on a Shimadzu UV-2600 spectrophotometer, and fluorescence excitation and emission spectra were recorded on the Hitachi F-7000 spectrofluorometer using a 10 mm path length cuvette at room temperature. LC-MS/MS spectra were recorded using a Shimadzu 8040 LC-MS spectrophotometer.

Chloro [1-((2-methyl)benzyl)-3-((anthracen-9-yl)methyl)benzimidazol-2-ylidene] silver(I), 2a. The ligand precursor (1-((2-methyl)benzyl)-3-((anthracen-9-yl)methyl)benzimidazolium chloride (**1a**) was synthesized according to procedure described in our previous study [14]. A methylene chloride (50 mL) mixture of **1a** (0.86 mmol, 387 mg) and silver(I) oxide (0.43 mmol, 100 mg) was stirred at room temperature for 72 h. After this period, the solution was filtered through Celite. The solvent was removed under vacuo, the crude product was washed with *n*-hexane (3 x 5 mL) and dried under reduced pressure. All manipulations during the synthesis, and storage of the solid was done in the absence of the light. Yellow solid, 445 mg (93 %). Melting point: 271–272 °C. Anal. Calcd. for $C_{30}H_{24}AgClN_2$: C, 64.82; H, 4.35; N, 5.04 %. Found: C, 64.27; H, 4.48; N, 4.97 %. ^{1}H NMR (400 MHz, $CDCl_3$): δ 8.64 (m, 1H, ArH), 8.29 (d, 2H, ArH, $J = 8.7$), 8.12 (d, 2H, ArH, $J = 8.6$), 7.60—7.51 (m, 4H, ArH), 7.20—7.02 (m, 7H, ArH), 6.62 (d, 1H, ArH, $J = 7.7$), 6.57 (s, 2H, –NC**H**$_2$C$_{14}$H$_9$), 5.57 (s, 2H, –NC**H**$_2$C$_6$H$_4$–2–CH$_3$), 2.34 (s, 3H, Ph–2–CH$_3$). ^{13}C NMR (100 MHz, $CDCl_3$): δ Carbene carbon was not detected, 135.4, 134.3, 134.1, 132.7, 131.5, 131.2, 130.9, 130.5, 130.1, 128.3, 127.8, 126.5, 126.2, 125.4, 124.4, 124.3, 123.2, 122.9, 112.2, 112.1, 51.9 (–N**C**H$_2$C$_{14}$H$_9$), 47.1 (–N**C**H$_2$C$_6$H$_4$–2–CH$_3$), 19.6 (Ph–2–CH$_3$). LC-MS (*m/z*): Anal. Calcd. for $C_{60}H_{48}AgN_4$ (Ag(NHC)$_2$) is 931.3; found is 932.0.

Chloro [1-((2-methoxy)ethyl)-3-((anthracen-9-yl)methyl)benzimidazol-2-ylidene] silver(I), 2b. The ligand precursor (1-((2-methoxy)ethyl)-3-((anthracen-9-yl)methyl)benzimidazolium chloride (**1b**) was synthesized according to procedure described in our previous study [14]. A methylene chloride (50 mL) mixture of **1b** (0.86 mmol, 347 mg) and silver(I) oxide (0.43 mmol, 100 mg) was stirred at room temperature for 72 h. After this period, the solution was filtered through Celite. The solvent was removed under vacuo, the crude product was washed with *n*-hexane (3 x 5 mL) and dried under reduced pressure. All manipulations during the synthesis, and storage of the solid was done in the absence of the light. Yellow solid, 312 mg (71 %). Melting point: 213–214 °C. Anal. Calcd. for $C_{25}H_{22}AgClN_2O$: C, 58.90; H, 4.35; N, 5.50 %. Found: C, 58.77; H, 4.59; N, 5.60 %. ^{1}H NMR (400 MHz, DMSO-d_6): δ 8.75 (s, 1H, ArH), 8.31 (d, 2H, ArH, $J = 8.5$), 8.14 (d, 2H, ArH, $J = 8.2$), 7.80 (d, 1H, ArH, $J = 7.9$), 7.70 (d, 1H, ArH, $J = 7.8$), 7.56–7.37 (m, 6H, ArH), 6.49 (s, 2H, –NC**H**$_2$C$_{14}$H$_9$), 4.35 (m, 2H, –CH$_2$C**H**$_2$OCH$_3$), 3.58 (m, 2H, –NC**H**$_2$CH$_2$OCH$_3$), 3.05 (m, 3H, –NCH$_2$CH$_2$OC**H**$_3$). ^{13}C NMR (100

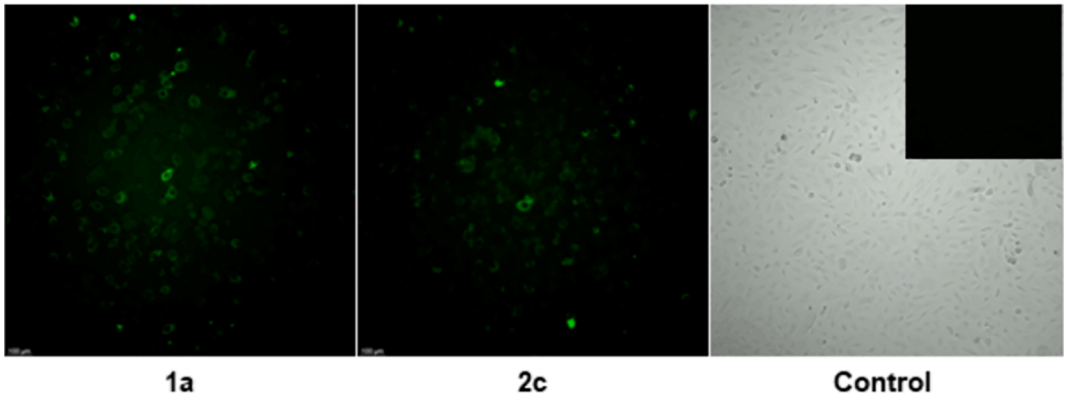

Fig. 5. Compounds **1a** and **2c**, and control were visualized using confocal microscopy. A549 cells were incubated with a concentration of 15.625 μM at 37 °C for 2 h.

MHz, DMSO-d_6): δ 188.4 (Ag–$C_{carbene}$), 134.3, 134.1, 131.5, 131.2, 130.01, 129.97, 127.8, 125.8, 125.4, 124.6, 124.4, 124.0, 112.9, 112.5, 71.1 (–NCH_2**C**H_2OCH_3), 58.7 (–NCH_2CH_2**O**CH_3), 49.5 (–**N**$CH_2C_{14}H_9$), 45.3 (–**N**$CH_2CH_2OCH_3$). LC-MS (*m/z*): Anal. Calcd. for $C_{50}H_{44}AgN_4O_2$ ($Ag(NHC)_2$) is 839.3; found is 840.0.

Bis(N-(((anthracen-9-yl)methyl)benzimidazole))silver(I) nitrate, 2c. N-(((anthracen-9-yl)methyl)benzimidazole) (**1c**) was synthesized according to procedure described in literature [10]. 1.18 mmol of **1c** was added into the suspension of silver nitrate (0.59 mmol, 100 mg) in ethanol (20 mL). The mixture was stirred for 4 h at 50 °C. After this period, the mixture was allowed to cool to ambient temperature. The precipitate formed was collected by filtration, washed with diethyl ether (3 x 10 mL) and dried under reduced pressure. All manipulations during the synthesis, and storage of the solid was done in the absence of the light. Yellow solid, 248 mg (54 %). Melting point: 236–238 °C. Anal. Calcd. for $C_{44}H_{31}AgN_5O_3$: C, 67.18; H, 4.10; N, 8.90 %. Found: C, 66.75; H, 4.41; N, 8.74 %. ^{1}H NMR (400 MHz, DMSO-d_6): δ 8.82 (s, 1H, ArH), 8.41 (d, 2H, ArH, $J = 8.2$), 8.22 (d, 2H, ArH, $J = 7.9$), 7.93 (d, 1H, ArH, $J = 8.1$), 7.86 (s, 1H, –NC**H**N–), 7.76 (d, 1H, ArH, $J = 8.0$), 7.62–7.57 (m, 4H, ArH), 7.43 (t, 1H, ArH, $J = 7.6$), 7.35 (t, 1H, ArH, $J = 7.6$), 6.57 (s, 2H, –NC**H**$_2C_{14}H_9$). ^{13}C NMR (100 MHz, DMSO-d_6): δ 144.9, 141.6, 133.6, 131.6, 131.1, 130.0, 129.9, 128.0, 126.0, 125.1, 124.4, 124.0, 123.7, 119.7, 112.2, 41.9 (–N**C**$H_2C_{14}H_9$). LC-MS (*m/z*): Anal. Calcd. for $C_{44}H_{32}AgN_4$ ($Ag(L)_2$) is 723.2; found is 723.0.

Chloro [(cyclooctadiene)(1-((2-methyl)benzyl)-3-((anthracen-9-yl)methyl))benzimidazol-2-ylidine] rhodium(I), 3a. A methylene chloride solution (20 mL) of **2a** (0.22 mmol, 120 mg) and $[RhCl(COD)]_2$ dimer (0.11 mmol, 54 mg) was stirred at room temperature for 24 h in the absence of light. After this period, the cleas solution was seperated from silver chloride precipitate by filtration through Celite. The solvent was removed under vacuo, the crude product was washed with *n*-hexane (3 x 5 mL) and dried under reduced pressure. Yellow solid, 95 mg (67 %). Melting point: 154–155 °C. Anal. Calcd. for $C_{38}H_{36}ClN_2Rh$: C, 69.25; H, 5.51; N, 4.25 %. Found: C, 68.82; H, 5.90; N, 4.27 %. ^{1}H NMR (400 MHz, $CDCl_3$): δ 8.72 (d, 2H, ArH, $J = 8.6$), 8.59 (s, 1H, ArH), 8.07 (d, 2H, ArH, $J = 8.4$), 7.62–7.49 (m, 5H, 4H are ArH and 1H is –NC**H**$_2C_{14}H_9$ as a geminal hydrogen), 7.30–7.18 (m, 2H, ArH), 7.04 (t, 1H, ArH, $J = 7.5$), 6.85–6.80 (m, 4H, 2H are ArH, 1H is –NC**H**$_2C_{14}H_9$ as a geminal hydrogen and 1H is –NC**H**$_2C_6H_4$-2-CH_3 as a geminal hydrogen), 6.71 (d, 1H, ArH, $J = 7.5$), 6.51 (t, 1H, ArH, $J = 7.5$), 6.03 (d, 1H, ArH, $J = 8.3$), 5.80 (d, 1H, –C**H**$_2C_6H_4$-2-CH_3 as a geminal hydrogen, $J = 16.6$), 5.22 (m, 2H, CH_{cod}), 3.64 (m, 1.H, CH_{cod}), 3.35 (m, 1H, CH_{cod}), 2.65 (s, 3H, Ph–2–CH_3), 2.40–2.21 (m, 3H, CH_{2cod}), 1.91 (m, 4H, CH_{2cod}), 1.78 (m, 1H, CH_{2cod}). ^{13}C NMR (100 MHz, $CDCl_3$): δ 197.8 (Rh–$C_{carbene}$, $J_{Rh\text{-}C}$ = 51.0), 135.5, 135.1, 134.8, 134.7, 131.6, 131.4, 130.5, 129.5, 129.3, 127.4, 126.3, 125.7, 125.4, 125.1, 124.7, 122.3, 122.1, 111.2, 110.5, 100.5 and 100.4 (two CH_{cod}, $J_{Rh\text{-}C} = 6.6$), 70.3 and 68.7, CH_{cod}, $J_{Rh\text{-}C}$ = 14.3), 50.4 (–N**C**$H_2C_{14}H_9$), 48.2 (–N**C**$H_2C_6H_4$-2-CH_3), 32.9, 32.7, 28.9 and 28.3 (four CH_{2cod}), 19.8 (Ph–2–CH_3). LC-MS (*m/z*): Anal. Calcd. for $C_{38}H_{36}ClN_2Rh$ ([Rh(NHC)Cl]) is 623.2; found is 623.0.

Chloro [(cyclooctadiene)(1-((2-methyl)benzyl)-3-((anthracen-9-yl)methyl))benzimidazol-2-ylidine] iridium(I), 4a. A methylene chloride solution (20 mL) of **2a** (0.22 mmol, 120 mg) and $[IrCl(COD)]_2$ dimer (0.11 mmol, 73 mg) was stirred at room temperature for 24 h in the absence of light. After this period, the cleas solution was seperated from silver chloride precipitate by filtration through Celite. The solvent was removed under vacuo, the crude product was washed with *n*-hexane (3 x 5 mL) and dried under reduced pressure. Orange solid, 68 mg (42 %). Melting point: 159–162 °C. Anal. Calcd. for $C_{38}H_{36}ClIrN_2$: C, 60.99; H, 4.85; N, 3.74 %. Found: C, 60.78; H, 5.33; N, 3.97 %. ^{1}H NMR (400 MHz, $CDCl_3$): δ 8.63 (d, 2H, ArH, $J = 8.8$), 8.49 (s, 1H, ArH), 7.98 (d, 2H, ArH, $J = 8.4$), 7.55–7.51 (m, 2H, ArH), 7.44–7.41 (m, 3H, 2H are ArH and 1H is –NC**H**$_2C_{14}H_9$ as a geminal hydrogen), 7.19–7.10 (m, 2H, ArH), 6.97 (t, 1H, ArH, $J = 7.5$), 6.77–6.71 (m, 3H, ArH), 6.61 (d, 1H, –C**H**$_2C_{14}H_9$ as a gemian hydrogen, $J = 15.1$), 6.45–6.41 (m, 2H, 1H is ArH and 1H is –C**H**$_2C_6H_4$-2-CH_3 as a geminal hydrogen), 5.95 (d, 1H, ArH, $J = 8.5$), 5.69 (d, 1H, –NC**H**$_2C_6H_4$-2-CH_3 as a gemina hydrogen, $J = 16.5$), 4.75 (m, 2H, CH_{cod}), 3.24 (m, 1H, CH_{cod}), 2.89 (m, 1H, CH_{cod}), 2.24–2.01 (m, 3H, CH_{2cod}), 1.74–1.55 (m, 4H, CH_{2cod}), 1.42 (m, 1H, CH_{2cod}), 2.51 (s, 3H, Ph-2-CH_3). ^{13}C NMR (100 MHz, $CDCl_3$): δ 193.1 (Ir–$C_{carbene}$), 135.5, 135.1, 134.8, 134.5, 131.6, 131.3, 130.4, 129.5, 129.3, 127.4, 126.3, 125.9, 125.4, 124.9, 124.7, 124.6, 122.4, 122.2, 111.4, 110.6, 87.5, 87.4, 54.0 and 52.4 (four CH_{cod}), 50.0 (–N**C**$H_2C_{14}H_9$), 47.9 (–N**C**$H_2C_6H_4$-2-CH_3), 33.5, 33.4, 29.5 and 28.9 (four CH_{2cod}), 19.8 (Ph–2–CH_3). LC-MS (*m/z*): Anal. Calcd. for $C_{38}H_{36}ClIrN_2$ ([Ir(NHC)Cl]) is 713.3; found is 713.0.

4.2. X-ray crystallography

Single crystal X-ray diffraction data of the compounds were obtained at room temperature using a Bruker D8 QUEST diffractometer equipped with Mo Kα radiation and a PHOTON III C14 detector. The data were collected, edited and parameterized by the APEX2 and SAINT [21]. The structures were solved by a dual-space algorithm using SHELXT-2018 [22] and refined with full-matrix least-squares calculations on F^2 using SHELXL-2019 [23]. All H atoms were located in difference maps and then treated as riding atoms. Crystal data, data collection and structure refinement details are given in Table S1. Molecular graphics were created by using OLEX2 [24].

4.3. Cytotoxicity studies

Cell Freezing Process: Cells grown in a monolayer are detached using trypsin and collected via centrifugation. Cryotubes are prepared, and a medium-DMSO mixture is added to protect cells from freezing damage. The tubes are frozen at −80 °C for long-term storage.

Dissolution and Recovery: Frozen cells in cryotubes are transferred to a 37 °C environment to thaw. Medium is quickly added to mitigate the impact of DMSO. Thawed cells are transferred to a centrifuge tube, additional medium is added, and centrifugation separates DMSO and residual components. The resulting pellet is cultivated in flasks with fresh medium.

Propagation and Passage of A549 Cells: A549 cells are cultured in flasks using Dulbecco's modified Eagle's medium (DMEM) medium. The cells are maintained by changing the medium every two days under controlled conditions. For passage, cells are detached using trypsin, suspended, centrifuged, resuspended, and then inoculated into fresh medium in flasks.

Cell Count and MTT Assay: Cell counts are performed using the CedexXs instrument with trypan blue before seeding cells into plates. The MTT assay assesses cell viability by measuring mitochondrial activity through conversion of a tetrazolium salt into a colored formazan crystal. These processes are crucial for maintaining cell viability, proper growth, and accurate experimental results in laboratory settings.

The cell line used in this study, human lung adenocarcinomic alveolar basal epithelial cell line A549, was obtained from the American Type Culture Collection (ATCC). A549 cell were seeded in a 96-well plate at 12.500 cell/well density. A549 cells were maintained in DMEM. Cell cultures were supplemented with 10 % fetal bovine serum (FBS), 2 mM L-glutamine, 10.000 units/mL penicillin and 10 mg/mL streptomycin and maintained at 37 °C in an atmosphere of 5 % CO_2 with 90 % relative humidity according to standard protocols [25]. The antiproliferative effect of the compounds (**1a, 2a, 3a, 4a, 2b, 2c**) was evaluated using the MTT reduction assay. Cells were treated with concentrations ranging from 0 to 62.5 μM of the compounds, which were dissolved in 5 % DMSO. The final concentration of DMSO in wells during compound treatment was 0.1 %. The treatment was conducted in mediums without phenol red, supplemented with 10 % FBS, for a duration of 24 h. Afterward, cells were rinsed three times with ice-cold PBS. MTT (3-(4,5-dimethylthiazol-2-yl)-2,5-diphenyltetrazolium bromide) was then added to a final concentration of 0.5 mg/mL. Following a 4-hour incubation with MTT, a solubilization buffer (10 % sodium dodecyl

sulfate in 0.01 mol/L HCl) was added, and the colored formazan crystals were gently re-suspended. The absorbance data at 570 nm were recorded using a microplate reader (Bio-Tek ELX800, BioTek Instruments Inc., Winooski, VT).

CRediT authorship contribution statement

Hatice Bekci: Resources, Investigation. **Namık Özdemir:** Software, Investigation, Data curation. **Zeynel Şahin:** Investigation, Data curation. **Akın Mumcu:** Investigation, Data curation. **Serkan Dayan:** Writing – original draft, Methodology, Investigation, Conceptualization. **Mert Olgun Karataş:** Writing – original draft, Methodology, Investigation, Conceptualization.

Declaration of competing interest

The authors declare that they have no known competing financial interests or personal relationships that could have appeared to influence the work reported in this paper.

Data availability

Data will be made available on request.

Acknowledgement

The authors acknowledge to Scientific and Technological Research Application and Research Center, Sinop University, Turkey, for the use of the Bruker D8 QUEST diffractometer.

Appendix A. Supplementary data

Supplementary data to this article can be found online at https://doi.org/10.1016/j.poly.2024.117011.

References

[1] (a) B. Rosenberg, L. Vancamp, T. Krigas, Nature 205 (1965) 698–699;
(b) B. Rosenberg, L. Vancamp, J.E. Trosko, V.H. Mansour, Nature 222 (1969) 385.
[2] A.L. Noffke, A. Habtemariam, A.M. Pizarro, P.J. Sadler, Chem. Commun. 48 (2012) 5219–5246.
[3] (a) W.A. Herrmann, Angew. Chem. Int. Ed. 41 (2002) 1290–1309;
(b) C.M. Crudden, D.P. Allen, Coord. Chem. Rev. 248 (2004) 2247–2273;
(c) E.A.B. Kantchev, C.J. O'Brien, M.G. Organ, Angew. Chem. Int. Ed. 46 (2007) 2768–2813;
(d) H. Jakobsen, A. Correa, A. Poater, C. Costabile, L. Cavallo, Coord. Chem. Rev. 253 (2009) 687–703.
[4] (a) K.M. Hindi, M.J. Panzner, C.A. Tessier, C.L. Cannon, W.J. Youngs, Chem. Rev. 109 (2009) 3859–3884;
(b) A. Gauiter, F. Cisnetti, Metallomics 4 (2012) 23–32;
(c) L. Oehninger, R. Rubbiani, I. Ott, Dalton Trans. 42 (2013) 3269–3284;
(d) S.B. Aher, P.N. Muskawar, K. Thenmozhi, P.R. Bhagat, Eur. J. Med. Chem. 81 (2014) 408–419;
(e) W. Liu, R. Gust, Coord. Chem. Rev. 329 (2016) 191–213.(f)S. A. Patil, A. P. Hoagland, S. A: Patil, A. Bugarin, Future Med. Chem., 2020, 12, 24.
[5] E. Peris, Chem. Rev. 118 (2018) 9988–10031.
[6] V.-W.-W. Yam, J.-K.-W. Lee, C.-C. Ko, N. Zu, J. Am. Chem. Soc. 131 (2009) 912–913.
[7] S.L. Balof, K.O. Nix, M.S. Olliff, S.E. Roessler, A. Saha, K.B. Müller, U. Bahrens, E. J. Valente, H.-S. Schanz, Beilstein J. Org. Chem. 11 (2015) 1960–1972.
[8] (a) M.E. Garner, W. Niu, X. Chen, I. Ghiviriga, K.A. Abboud, W. Tan, A.S. Veige, Dalton Trans. 44 (2015) 1914–1923;
(b) O. Dada, G. Sanzhez-Sanz, M. Tacke, X. Zhu, Tetrahedron Lett. 59 (2018) 2904–2908;
(c) M.O. Karataş, G. Çalgın, B. Alıcı, B. Gökçe, N. Gencer, T.T. Tok, O. Arslan, I. Kılıç-Cıkla, N. Özdemir, Appl. Organomet. Chem. 33 (2019) e5130.
[9] Y. Inagaki, T. Kokudo, M. Kamiya, S. Uno, M. Sato, J. Kaneko, N. Kokudo, Y. Urano, K. Hasegawa, Sci. Rep. 9 (2019) 3044.
[10] (a) A. Citta, E. Schuh, F. Mohr, A. Folda, M.L. Massimino, A. Bindoli, A. Casini, M. P. Rigobello, Metallomics 5 (2013) 1006–1015;
(b) T. Zou, C.T. Lum, S.-S.-Y. Chui, C.-M. Che, Angew. Chem. Int. Ed. 52 (2013) 2930–2933;
(c) B. Bertrand, A. de Almeida, E.P.M. van der Burgt, M. Picquet, A. Citta, A. Folda, M.B. Rigobello, P. Le Gendre, E. Bodio, A. Casini, Eur. J. Inorg. Chem. (2014) 4532–4536;
(d) K.M. Groves, C.F. Williams, A.J. Hayes, B.D. Ward, M.D. Isaacs, M.O. Symonds, D. Lloyd, P.N. Horton, S.J. Coles, S.J.A. Pope, Dalton Trans. 48 (2019) 1599–1612;
(e) M.G. Fabbrini, D. Cirri, A. Pratesi, L. Ciofi, T. Marzo, A. Guerri, S. Nistri, A. Dell'Accio, T. Gamberi, M. Severi, A. Bencini, L. Messori, ChemMedChem 14 (2019) 182–188;
(f) F. Guarra, N. Busto, A. Guerri, L. Marchetti, T. Marzo, B. Garcia, T. Biver, C. Gabbiani, J. Inorg. Biochem. 205 (2020) 110998;
(g) F. Rong, B. Mienli, H. Lihong, W. Liu, Eur. J. Med. Chem. 183 (2019) 111721;
(h) W. Streciwilk, A. Terenzi, X. Cheng, L. Hager, Y. Dabiri, P. Prochnow, J. E. Bandow, S. Wölfl, B.K. Keppler, I. Ott, Eur. J. Med. Chem. 156 (2018) 148–161.
[11] (a) S. Harlepp, E. Chardon, M. Bounche, G. Dahm, M. Maaloum, S. Bellemin-Laponnaz, Int. J. Mol. Sci. 20 (2019) 4198;
(b) C.H.G. Jakob, B. Dominelli, J.F. Schlagintweit, P.J. Fischer, F. Schuderer, R. M. Reich, F. Marques, J.D.G. Correira, F.E. Kühn, Chem. Asia J. 15 (2020) 4275–4279;
(c) F. Binacchi, F. Guarro, D. Cirri, T. Marzo, A. Pratesi, L. Messori, C. Gabbiani, T. Biver, Molecules 25 (2020) 5446;
(d) B.Y.T. Lee, M.P. Sullivan, E. Yano, K.K.H. Tong, M. Hanif, T. Kawakubo-Yasukochi, S.M.F. Jamieson, T. Soehnel, D.C. Goldstone, C.G. Hartinger, Inorg. Chem. 60 (2021) 14636–14644.
[12] B.Y.T. Lee, A.D. Phillips, M. Hanif, K.K.H. Tong, T. Soehnel, C.G. Hartinger, Inorg. Chem. 60 (2021) 8734–8741.
[13] J.-Z. Fan, Z.-W. Wu, S. Bai, L.-F. Wang, Y.-F. Han, Organometallics 42 (2023) 1013–1020.
[14] M.O. Karatas, B. Alici, E. Cetinkaya, Ç. Bilen, N. Gençer, O. Arslan, Russ. J. Bioorg. Chem. 40 (2014) 461–466.
[15] (a) M. Barwiolek, A. Wojtczak, A. Kozakiewicz, R. Szcesny, M. Babinska, L. Skowronski, E. Szlyk, New J. Chem. 42 (2018) 18559–18568;
(b) D. Zyro, A. Sliwinska, I. Szymczak-Pajor, M. Strek, J. Ochocki, Cancers 12 (2020) 3848;
(c) K. Stryjska, L. Radko, L. Checinska, J. Kusz, A. Posyniak, J. Ochocki, Int. J. Mol. Sci. 21 (2020) 3629;
(d) M.O. Karataş, N. Özdemir, M. Sarıman, S. Günal, E. Ulukaya, İ. Özdemir, Dalton Trans. 50 (2021) 11596–11603;
(e) E. Arı, N. Şahin, E. Üstün, M. Dündar, H. Karci, İ. Özdemir, A. Koç, N. Gürbüz, İ. Özdemir, J. Biol. Inorg. Chem. 28 (2023) 725–736.
[16] (a) S. Saravanakumar, A.I. Oprea, M.K. Kindermann, P.G. Jones, J. Heinicke, Chem. Eur. J. 12 (2006) 3143–3154;
(b) P.V. Simpson, B.W. Skelton, D.H. Brown, M.V. Baker, Eur. J. Inorg. Chem. 12 (2011) 1937–1952;
(c) Q.-X. Liu, H. Wang, X.-J. Zhao, Z.-Q. Yao, Z.-Q. Wang, A.-H. Chen, X.-G. Wang, CrystEngComm. 14 (2012) 5330–5348;
(d) J.T. Price, N.D. Jones, P.J. Ragogna, Inorg. Chem. 51 (2012) 6776–6783;
(e) R. Kishore, S.K. Das, J. Mol. Struct. 1053 (2013) 38–47;
(f) Y. Gök, S. Akkoç, S. Albayrak, M. Akkurt, M.N. Tahir, Appl. Organomet. Chem. 28 (2014) 244–251;
(g) N. Şahin, S. Şahin-Bölükbaşı, M.N. Tahir, C. Arıcı, E. Çevik, N. Gürbüz, İ. Özdemir, B.S. Cummings, J. Mol. Struct. 1179 (2019) 92–99;
(h) S. Şahin-Bölükbaşı, N. Şahin, M.N. Tahir, C. Arıcı, E. Çevik, N. Gürbüz, İ. Özdemir, B.S. Cummings, Inorg. Chim. Acta 486 (2019) 711–718;
(i) S.D. Düşünceli, D. Ayaz, E. Üstün, S. Günal, N. Özdemir, M. Dinçer, İ. Özdemir, J. Coord. Chem. 73 (2020) 1967–1986.
[17] L. Yang, D.R. Powell, R.P. Houser, Dalton Trans. 9 (2007) 955–964.
[18] A. Okuniewski, D. Rosiak, J. Chojnacki, B. Becker, Polyhedron 90 (2015) 47–57.
[19] (a) A. Zanardi, E. Peris, J.A. Mata, New. J. Chem. 32 (2008) 120–126;
(b) A. Azua, J.A. Mata, E. Peris, F. Lamaty, J. Martinez, E. Colacino, Organometallics 31 (2012) 3911–3919;
(c) M.O. Karataş, T. Keskin, N. Özdemir, H. Küçükbay, S. Tekin, A. Mansur, S. Günal, S. Sandal, Inorg. Chem. Commun. 146 (2022) 110080.
[20] (a) H. Varbanov, S.M. Valiahdi, A.A. Legin, M.A. Jakupec, A. Roller, M. S. Galanski, B.K. Keppler, Eur. J. Med. Chem. 46 (2011) 5456–5464;
(b) N. Sarin, F. Engel, G.V. Kalayda, M. Mannewitz, J. Cinatl, F. Rothwieler, M. Michaelis, H. Saafan, C.A. Ritter, U. Jaehde, R. Frötschl, Plos One 12 (2017) e0181081.
[21] Bruker (2013). APEX2 and SAINT. Bruker AXS Inc., Madison, Wisconsin, USA.
[22] G.M. Sheldrick, Acta Crystallogr. A 71 (2015) 3–8.
[23] G.M. Sheldrick, Acta Crystallogr. C 71 (2015) 3–8.
[24] O.V. Dolomanov, L.J. Bourhis, R.J. Gildea, J.A.K. Howard, H. Puschmann, J. Appl. Crstallogr. 42 (2009) 339–341.
[25] (a) A. Cumaoglu, S. Dayan, A.O. Agkaya, Z. Ozkul, N.K. Ozpozan, J. Enzyme Inhib. Med. Chem. 30 (2015) 413–419;
(b) A.O. Agkaya, S. Dayan, Z. Ozkul, N.K. Ozpozan, A. Cumaoglu, Med. Chem. Res. 24 (2015) 3972.